

# VLT-ISAAC near-IR Spectroscopy of ISO selected Hubble Deep Field South Galaxies<sup>12</sup>

D. Rigopoulou<sup>1</sup>, A. Franceschini<sup>2</sup>, H. Aussel<sup>3</sup>, R. Genzel<sup>1</sup>, P. van der Werf<sup>4</sup>, C.J. Cesarsky<sup>5</sup>, M. Dennefeld<sup>6</sup>, S. Oliver<sup>7</sup>, M. Rowan-Robinson<sup>7</sup>, R. Mann<sup>8</sup>, I. Perez-Fournon<sup>9</sup>,  
B. Rocca-Volmerange<sup>6</sup>

Received \_\_\_\_\_; accepted \_\_\_\_\_

---

<sup>1</sup>Max-Planck-Institut für extraterrestrische Physik, Postfach 1312, 85741 Garching, Germany

<sup>2</sup>Dipartimento di Astronomia, Università di Padova, Vicolo Osservatorio 5 I-35122, Padova, Italy

<sup>3</sup>Osservatorio Astronomico di Padova, Vicolo Osservatorio 5 I-35122, Padova, Italy

<sup>4</sup>Leiden Observatory, PO Box 9513, 2300 RA, Leiden, The Netherlands

<sup>5</sup>European Southern Observatory, Karl-Schwarzschild-str. 2, 85740 Garching, Germany

<sup>6</sup>Institut d'Astrophysique de Paris - CNRS, 98 bis Boulevard Arago, 75014 Paris, France

<sup>7</sup>ICSTM, Astrophysics Group, Blackett Laboratory, Prince Consort Rd., London, SW2 1BZ, U.K.

<sup>7</sup>Institute for Astronomy, University of Edinburgh, Royal Observatory, Blackford Hill, Edinburgh, EH9 3NJ, UK

<sup>9</sup>Instituto de Astrofísica de Canarias, Via Lactea s/n, 38200 La Laguna, Tenerife, Spain

## ABSTRACT

We report the results of near-infrared VLT-ISAAC spectroscopy of a sample of 12 galaxies at  $z = 0.4\text{--}1.4$ , drawn from the ISOCAM survey of the Hubble Deep Field South. We find that the rest frame R-band spectra of the ISOCAM galaxies resemble those of powerful dust-enshrouded starbursts.  $H_\alpha$  emission is detected in 11 out of 12 objects down to a flux limit of  $7 \times 10^{-17}$  erg cm $^{-2}$  s $^{-1}$ , corresponding to a luminosity limit of  $10^{41}$  erg s $^{-1}$  at  $z = 0.6$ , (for an  $H_0 = 50$  and  $\Omega = 0.3$  cosmology). From the  $H_\alpha$  luminosities in these galaxies we derive estimates of the star formation rate in the range  $2\text{--}50$  M $_\odot$ /yr for stellar masses  $1\text{--}100$  M $_\odot$ . The raw  $H_\alpha$ -based star formation rates are an order of magnitude or more lower than SFR(FIR) estimates based on ISOCAM LW3 fluxes. If the  $H_\alpha$  emission is corrected for extinction the median offset is reduced to a factor of 3. The sample galaxies are part of a new population of optically faint but infrared-luminous active starburst galaxies, which are characterized by an extremely high rate of evolution with redshift up to  $z \sim 1.5$  and expected to contribute significantly to the cosmic far-IR extragalactic background.

*Subject headings:* galaxies: evolution - galaxies: starburst - cosmology: observations

---

<sup>1</sup>Based on observations with ISO, an ESA project with instruments funded by ESA member states (especially the PI countries: France, Germany, the Netherlands, and the United Kingdom) with the participation of ISAS and NASA.

<sup>2</sup>Based on observations collected at the European Southern Observatory, Chile, ESO No 63.O-0022

## 1. Introduction

Until recently, most of our knowledge about high- $z$  galaxies has come from optical surveys. The COBE detection of an extragalactic far-infrared/submm background (Puget et al. 1996), with an integrated intensity similar to or greater than that of optical light (e.g. Hauser et al. 1998), strongly suggests that a significant fraction of the cosmic star formation in the Universe is obscured by dust and thus missed by the various optical surveys.

With the advent of the Infrared Space Observatory (ISO, Kessler et al. 1996) deep mid-IR surveys for distant galaxies, have been successfully carried out for the first time. Operating in the  $5 - 18 \mu\text{m}$  band sensitive to warm dust and emission from Polycyclic Aromatic Hydrocarbons (PAH), ISOCAM on board ISO was more than 1000 times more sensitive than IRAS and thus had the potential to study infrared bright galaxies at redshifts beyond 0.5. A number of cosmological surveys have been performed with ISOCAM especially in the LW3 filter ( $12 - 18\mu\text{m}$ ). These surveys range from the wide and shallow European Large Area ISO Survey (ELAIS, Oliver et al. 2000), to deep pencil-beam surveys in the Lockman Hole, the Marano field, the Northern and Southern Hubble Deep Fields (HDF-N, HDF-S) and the distant cluster Abell 2390, reaching limiting flux densities of  $50 - 100 \mu\text{Jy}$  (Elbaz et al. 1999).

At the bright end the ISOCAM source counts combined with those of IRAS are in good agreement with no or moderate evolution. At fainter flux densities the counts steepen considerably and at  $\sim 200 - 600 \mu\text{Jy}$  they are about an order of magnitude greater than the predictions of no evolution models. This steepening in the  $\log N - \log S$  plot and a pronounced maximum in the differential number counts at  $\sim 400 \mu\text{Jy}$  suggest that the ISOCAM surveys have revealed a population of strongly evolving galaxies. Elbaz et al. (2000, in preparation) show that this population plausibly accounts for a significant fraction of the far-IR background. The next step is to explore the nature of the ISOCAM population

with optical/near-IR spectroscopy. In this letter we report on the first near-IR (rest-frame R-band) spectroscopic survey of a representative sample of faint ISOCAM galaxies in the HDF-S field.

## 2. Sample Selection

The HDF-S was observed by ISOCAM as part of the ELAIS survey. The observations were carried out at two wavelengths, LW2 (6.75  $\mu\text{m}$ ) and LW3 (15  $\mu\text{m}$ ). Oliver et al. (2000, in preparation) and Aussel et al. (2000, in preparation) analyzed the data independently. Aussel et al. used the PRETI method and detected 63 sources brighter than  $S_{15\mu\text{m}} = 100 \mu\text{Jy}$  in the LW3 band. We used this source list as input for our observations.

We selected the sample for ISAAC follow up from the HDF-S LW3 sources based on the following criteria: a) a reliable LW3 detection, b)  $H_\alpha$  in the wavelength range of ISAAC and, c) a secure counterpart in the I band image (Dennefeld et al. 2000, in preparation), or a counterpart in the K band image (ESO Imaging Survey (EIS) Deep). We did not apply any selection based on colors. Our reference sample contains 25 galaxies with 15  $\mu\text{m}$  flux densities ranging between 100–800  $\mu\text{Jy}$ . It is thus a fair representation of the strongly evolving ISOCAM population near the peak of the differential source counts (Elbaz et al. 1999). From these 25 optically identified sources we randomly selected 12 sources for ISAAC-follow up. To select the near-IR band (Z, SZ, J, H) for our spectroscopy we used spectroscopic redshifts from optical spectroscopy, where available, for  $z < 0.7$  (Dennefeld et al. 2000, in prep.). Otherwise we used photometric redshift estimates based on the model PEGASE (Fioc and Rocca-Volmerange 1997). Our photometric redshift determinations turned out to be accurate to  $\Delta z \pm 0.1$ .

### 3. Observations and Results

We collected the spectra during 1999 September 20–24 with the infrared spectrometer ISAAC (Moorwood et al. 1998) on the ANTU–ESO telescope (formerly UT1), on Paranal, Chile. For the observations we used the low resolution grating  $R_s \sim 600$  and a  $1'' \times 2'$  long slit. To maximize the observing efficiency each slit position included on average two galaxies at any given orientation. Most of the targets were first acquired directly from a 1–2 min exposure in the H-band. In the case of the very faint objects ( $H \geq 20.0$  mag) we offset from a brighter star in the HDF-S field. Observations were made by nodding the telescope  $\pm 20''$  along the slit to facilitate sky subtraction (always avoiding overlap of the two objects in the slit). Individual exposures ranged from 2–4 minutes. Sky conditions were excellent throughout the acquisition of the spectra, with seeing values in the range  $0.4''$ – $1.0''$ . For each filter, observations of spectroscopic standard stars were made in order to flux calibrate the galaxy spectra.

The data were reduced using applications from ECLIPSE (Devillard 1998) and IRAF packages. Accurate sky subtraction is critical to the detection of faint lines. Sky was removed by subtracting the pairs of offset frames. In some cases this left a residual signal (due to temporal sky changes) which was then removed by performing a polynomial interpolation along the slit. OH sky emission lines were also carefully removed from the spectra. Spectrum extraction for each galaxy was performed using the APEXTRACT package. Standard wavelength calibration was applied.

The spectra for all 12 galaxies observed with ISAAC are shown in Figure 1. Table 1 contains exposure times,  $H_{AB}$  magnitudes, measured spectroscopic redshifts (from  $H_\alpha$  detections),  $H_\alpha$  line fluxes and Equivalent Widths (EW) (and where resolved [NII] fluxes). We convert the  $H_\alpha$  line fluxes to luminosities using  $H_0 = 50 \text{ km s}^{-1} \text{ Mpc}^{-1}$  and  $\Omega = 0.3$ . We also list in Table 1 FIR luminosities based on LW3 fluxes (see Section 5 for more details).

We note that we have not detected any  $H_\alpha$  Broad Line components.

#### 4. The nature of the ISOCAM faint galaxies: Dusty and Luminous Starbursts

Prior to our study no near-infrared (rest-frame R-band) spectroscopy had been carried out for the ISOCAM population, primarily because of the faintness of the galaxies. Aussel et al. (1999) and Flores et al. (1999) have presented optical spectroscopic analysis (rest-frame B-band) for HDF-N and the 1415+52 field of the Canada-France Redshift Survey (CFRS), respectively. Aussel et al. (1999) cross-correlated the ISOCAM HDF-N galaxies with the optical catalog of Barger et al. (1999) resulting in 38 galaxies with confirmed spectroscopic redshifts. Flores et al. have identified 22 galaxies with confirmed spectroscopic information. In both of these samples the median redshift is about 0.7. Our ISOHDFS sample contains 7 galaxies  $0.4 < z < 0.7$  and 5 galaxies with  $0.7 < z < 1.4$  and thus, has a  $z$ -distribution very similar to the HDF-N (Aussel et al.) and CFRS (Flores et al.) samples.

Rest-frame B-band spectra host a number of emission and absorption lines related to the properties of the starburst in the galaxy. Based on these features galaxies can be classified according to their starburst history. Strong  $H_\delta$ ,  $H_\epsilon$  Balmer absorption and no emission lines are characteristic of passively evolving k+A galaxies. The presence of Balmer absorption lines implies the presence of a dominating A-star population formed about 0.1–1 Gyr ago. The simultaneous presence of Balmer absorption and moderate flux [OII] and  $H_\beta$  emission termed as e(a) or S+A galaxies, indicates that, in addition, there is ongoing star formation. The relative importance of these star formation episodes depends on the extinction (especially of the current star formation component). If the extinction is low the galaxy is primarily a post–starburst system. If the extinction toward the star forming region is high then the galaxy could be a powerful starburst. The majority of the galaxies in the CFRS field ( $\sim 70\%$ ) display optical spectra characteristic of e(a) galaxies. As evidenced

by the detections in Figure 1, the ISOCAM galaxies are in fact powerful starbursts hidden by large amounts of dust extinction.

Remarkably, dusty starbursts such as M82 ( $L \sim 10^{10} L_{\odot}$ , Kennicutt et al. 1992), LIRGs (Luminous InfraRed Galaxies,  $L \sim 10^{11} L_{\odot}$ , Wu et al. 1998), and many bright ULIRGs ( $L \sim 10^{12} L_{\odot}$ , Liu and Kennicutt 1995), show e(a) B-band spectra. Local e(a) galaxies have large  $H_{\alpha}$  equivalent widths (EW), at the same time demonstrating active current star formation and differential dust extinction. The measured EW ratio ( $[OII]/H_{\alpha}$ ) for e(a) galaxies appears to be somewhat low. Such low ratios have already been observed in the spectra of distant clusters (Dressler et al. 1999), nearby mergers (Poggianti and Wu 2000), the dusty LIRGs studied by Wu et al. (1998) or the interacting/merging systems studied by Liu and Kennicutt (1995). The behaviour of the  $(OII)/(H_{\alpha}+NII)$  ratio is shown in the  $EW(OII)$ – $EW(H_{\alpha}+NII)$  diagram of Figure 2: the majority of the points lie below the straight line. For our ISOHDFS sample we use the  $EW(H_{\alpha})$  measured from the observations presented here. For the  $EW(OII)$  we use a median value of  $20 \pm 15 \text{ \AA}$  which was recently measured from FORS2 I-band spectra of a small sample of ISOHDFS galaxies (Franceschini et al. 2000, in preparation). This value is in agreement with the results presented by Flores et al. (1999) for the CFRS galaxies.

It follows from Figure 2 that the ISOHDFS galaxies occupy the same region in the  $EW(OII)/EW(H_{\alpha}+NII)$  diagram as actively starforming galaxies. Intrinsic differential dust extinction is responsible for the somewhat low  $EW(OII)/EW(H_{\alpha}+NII)$  ratio. The  $[OII]$  emission is affected more than  $H_{\alpha}$  simply because of its shorter wavelength. The continuum is due to A-stars which come from earlier (0.1–1.0 Gyr) star formation activity that is not energetically dominant and plays a small role once the dusty starburst is dereddened. This scenario implies that these galaxies undergo multiple burst events: the less extincted population is due to an older burst while in the heavily dust enshrouded HII regions there

is ongoing star formation. We conclude that ISOCAM galaxies are actively starforming, dust enshrouded galaxies, akin to local LIRGs (e.g. NGC 3256, Rigopoulou et al. 1996).

### 5. Star Formation Rates and Extinction Corrections

The conversion factor between ionizing luminosity and star formation rate (SFR) is usually computed using an evolutionary synthesis model. Only massive stars ( $> 20 M_{\odot}$ ) with short lifetimes ( $\leq 10^6$  yrs) contribute to the integrated ionizing flux. Using the stellar synthesis code STARS (Sternberg 1998) we create models for solar abundances, a Salpeter IMF (1–100  $M_{\odot}$ ) and slowly decaying bursts with ages in the range of a few  $\times 10^7$ – $10^8$  yrs, and SFR decay time-scales in the range  $10^7$ – $10^9$  yrs. Averaging, we obtain:

$$\text{SFR}(M_{\odot}/yr) = 5 \times 10^{-42} L_{H\alpha} (\text{erg s}^{-1}). \tag{1}$$

We have used this formula to estimate the SFR rates in Table 2. The SFR estimates based on Eqn.(1) are a factor of 1.6 smaller than the SFR estimates based on the Kennicutt (1998) relationship that refers to stars in the range 0.1–100  $M_{\odot}$ . Averaging over our models, the SFR scales with the FIR luminosity as:

$$\text{SFR}(M_{\odot}/yr) = 2.6 \times 10^{-44} L_{FIR} (\text{erg s}^{-1}) \tag{2}$$

Since extinction is at play, the SFR estimates we quote in the first column of Table 2 are *lower limits* to the real SFR in these galaxies. We derive the extinction based on V–K color indices (magnitudes taken from the EIS Survey). Using STARS as well as the Starburst99 (Leitherer et al. 1999) codes for various star formation histories (ie bursts of



different duration, and continuous star formation) we calculate the range of intrinsic colors. The model predicted intrinsic V–K colors are in the range 1.1 – 1.5. We have applied infrared and optical K-corrections from Poggianti (1997) and Coleman (1980), respectively. Comparing the observed V–K colors to the predicted ones we obtain a median color excess of 2.0 which corresponds to a median  $A_V$  of 1.8 assuming a screen model for the extinction. This  $A_V$  value corresponds to a median correction factor for the  $\text{SFR}(H_\alpha)$  of  $\sim 4$ .

The SFR can also be inferred from far-infrared (FIR) luminosities according to Eqn. (2). The  $\text{SFR}(\text{FIR})$  estimates in Table 2 are based on the method of Franceschini et al. (2000, in prep.) which makes use of the 15  $\mu\text{m}$  flux and assumes a  $L_{\text{FIR}}/L_{\text{MIR}}$  ratio of  $\sim 10$  (for an M82 like SED, Vigroux et al. 1999). The  $\text{SFR}(\text{FIR})$  estimates turn out to be a factor of 5 to 50 higher than the SFR estimates inferred from the *non-extinction corrected*  $H_\alpha$ . However, if we apply the correction factor of  $\sim 4$  we deduced for the  $H_\alpha$  then  $\text{SFR}(\text{FIR})/\text{SFR}(H_\alpha) \sim 3$ , confirming that the extinction is much higher than can be predicted using (UV or) optical observations. Thus, ISOCAM galaxies are in fact actively star forming highly dust enshrouded galaxies. One exception is source ISOHDFS 38 for which we have evidence for the presence of a dominant AGN component (both from the LW2/LW3 ratio and the  $H_\alpha/[\text{NII}]$  ratio).

Based on our SFR estimates, and the evidence for extinction presented in section 4.1 we conclude that ISOCAM galaxies are indeed dust enshrouded actively star-forming galaxies and not decaying post-starburst systems.

## 6. Conclusions

We have presented NIR spectroscopy, rest frame R-band, of a sample of ISO selected galaxies from the Hubble Deep Field South. We have detected  $H_\alpha$  emission in almost all of

them. The detections of the  $H_\alpha$  line combined with the large  $H_\alpha$  EWs are consistent with the idea that these galaxies are ongoing powerful dusty starbursts.

Using the observed  $H_\alpha$  emission lines we estimate that the SFR rate in the ISOHDFS galaxies ranges between 2 and 50  $M_\odot/\text{yr}$ , far higher than those inferred from local Starbursts (Calzetti 1997) and local spirals (Kennicutt 1992). We have compared these rates of SF with the values estimated from the FIR luminosities, which are typically a factor 5 to 50 larger because of dust obscuration. We estimated the  $H_\alpha$  extinction using standard extinction laws. The  $H_\alpha$  extinction corrected SFR estimates are then higher although still fall short of the SFR estimates based on FIR luminosities (  $\text{SFR}(\text{FIR}):50\text{--}400 M_\odot/\text{yr}$ ). This result demonstrates that it is very dangerous to derive star formation rates from UV or optical data alone since these wavelengths are susceptible to higher extinction. Thus a significant fraction of star formation is missed by optical surveys. We conclude that ISO has detected in the mid-IR the most active, luminous and dust-enshrouded starbursts at  $z \sim 0.4\text{--}1.4$ , which would have remained otherwise unnoticed by optical surveys. This population of strongly evolving active dusty starbursts is likely to account for a substantial fraction of the FIR/submm background (Elbaz et al. 2000, in preparation).

This work is supported by the EC TMR Network “European Large Area ISO Surveys” (contract No. ERBFMRX-CT96-0068). We thank the EC TMR Network “Galaxy Formation and Evolution ” for making redshift information available prior to publication. H.A. is supported by the TMR network “Galaxy formation and evolution”, contract No. ERBFRX-CT96-0086. We thank Amiel Sternberg for fruitful discussions.

## REFERENCES

- Aussel, H., Cesarsky, C.J., Elbaz, D., Starck, J.L., 1999 A&A 342, 313
- Barger, A.J., Cowie, L.L., Trentham, N., Fulton, et al., 1999 AJ 117, 102
- Calzetti, D., 1997, AJ, 113, 162
- Coleman, G.D., Chi-Chao, W., Weedman, D.W., 1980, ApJS 43, 393
- Fioc, M., Rocca-Volmerange, B., 1997, A&A 326, 950
- Flores, H., Hammer, F., Thuan, T.X., Cesarsky, C., 1999, Ap.J., 517, 148
- Dressler, A., Smail, I., Poggianti, B.M., Butcher, H., et al. 1999, astro-ph/9901263
- Elbaz, D., Cesarsky, C.J., Fadda, D., Aussel, H., et al., 1999, A&A 351, L37
- Hauser, M.G., Arendt, R.G., Kelsall, T., 1998, ApJ 481, 49
- Kennicutt, R.C., 1992, Ap.J., 388, 310
- Kennicutt, R.C., 1998, Ann. rev. Astr. Ap. 36, 189
- Kessler, M.F., et al., 1996, A&A 315, L27
- Leitherer, C., et al., 1999, ApJS 123, 3
- Liu, C.T., Kennicutt, R.C., 1995, Ap.J., 450, 547
- Moorwood, A.F.M., et al., 1998, Msng 74, 7
- Poggianti, B.M., 1997, A&A Suppl. 122, 399
- Poggianti, B.M., Wu, H., 2000, Ap.J. 529, 157

Puget, J-L., Abergel, A., Bernard J-P., Boulanger, F., Burton W.B., et al., 1996, A&A 308,  
L5

Oliver, S., et al., 2000, MNRAS, in press

Rigopoulou, D., et al, 1996, A&A, 305, 747

Sternberg, A., 1998, ApJ, 506, 721

Vigroux, L., et al. 1999, in : “The Universe as seen by ISO” eds. P. Cox and M.F. Kessler,  
ESA SP-427, 805

Wu, H., Zou, Z.L., Xia, X.Y., Deng, Z.G., 1998, A&AS, 127, 521

## FIGURES

Fig. 1.— ISOHDFS-VLT spectra

Fig. 2.—  $EW(OII) - EW(H_{\alpha} + NII)$

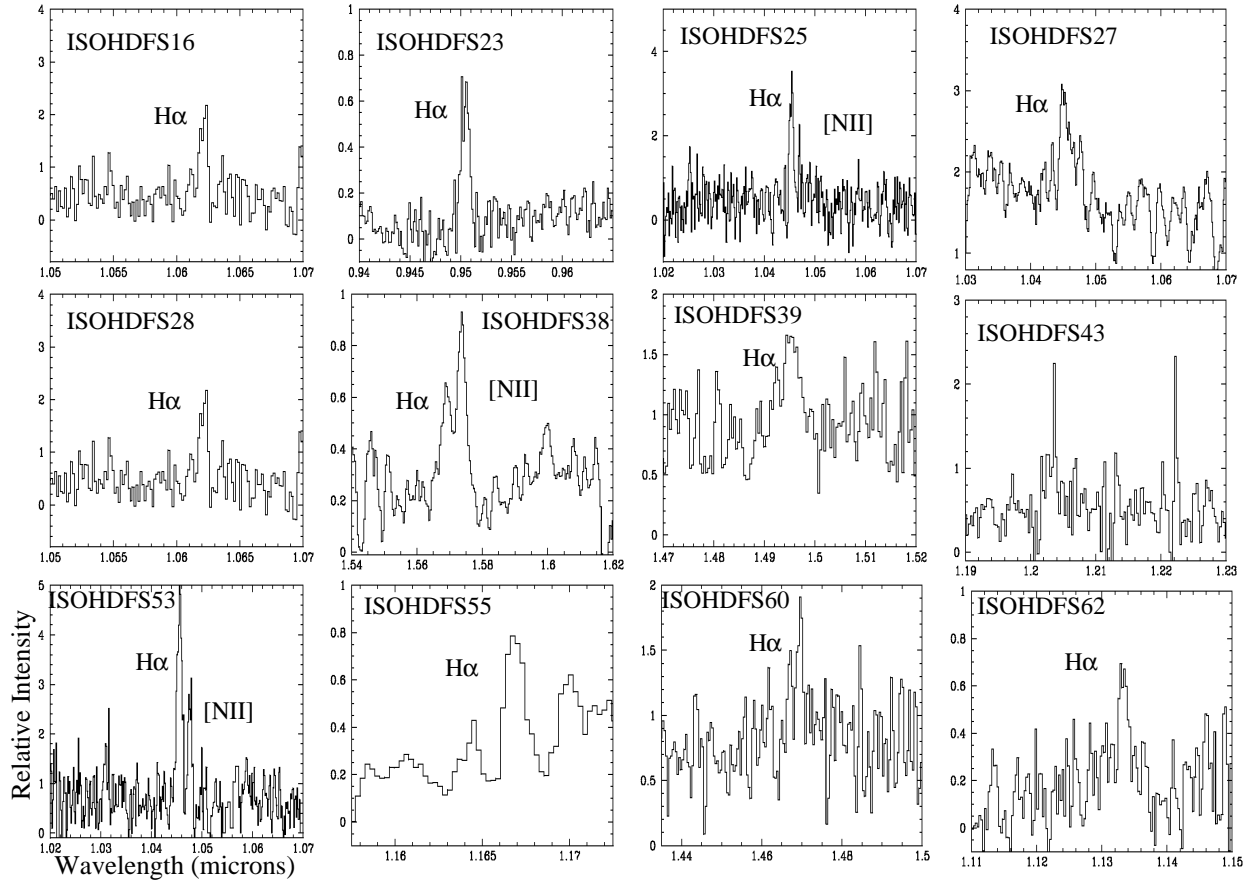


Fig. 1.— ISAAC-VLT spectra. The  $H_{\alpha}$  and  $[NII]$  (wherever resolved) lines are indicated.

Table 1. ISOHDFS sample and flux measurements

| name                   | Exp.  | $z_{spec}$ | Hmag  | F( $H_\alpha$ ) <sup>1</sup> | EW( $H_\alpha$ + $[NII]$ ) | L( $H_\alpha$ ) | L(FIR) |
|------------------------|-------|------------|-------|------------------------------|----------------------------|-----------------|--------|
|                        | (sec) |            | (mag) | F( $[NII]$ ) <sup>1</sup>    | EW( $[NII]$ )              |                 |        |
|                        |       |            |       |                              | Å                          |                 |        |
| ISOHDFS16              | 3720  | 0.62       | 20.73 | 1.17                         | 45                         | 0.29            | 0.54   |
| ISOHDFS23              | 3720  | 0.46       | 19.26 | 1.86                         | 50                         | 0.23            | 2.5    |
| ISOHDFS25              | 3720  | 0.59       | 19.80 | 3.12                         | 110 <sup>5</sup>           | 0.67            | 2.0    |
|                        |       |            |       | 0.72                         | 35                         |                 |        |
| ISOHDFS27              | 3720  | 0.58       | 18.39 | 3.28                         | 47                         | 0.71            | 1.61   |
| ISOHDFS28              | 3720  | 0.56       | 20.36 | 0.78                         | 47                         | 0.16            | 0.77   |
| ISOHDFS38              | 7400  | 1.39       | 21.67 | 1.95                         | 35 <sup>5</sup>            | 3.62            | 23.0   |
|                        |       |            |       | 4.22                         | 50                         |                 |        |
| ISOHDFS39              | 7400  | 1.27       | 20.95 | 7.13                         | 67                         | 10.4            | 6.15   |
| ISOHDFS43 <sup>4</sup> | 3720  | –          | 21.92 | –                            | –                          | –               | –      |
| ISOHDFS53              | 3720  | 0.58       | 19.47 | 6.08                         | 70 <sup>5</sup>            | 1.32            | 1.53   |
|                        |       |            |       | 2.8                          | 50                         |                 |        |
| ISOHDFS55              | 3720  | 0.76       | 20.05 | 2.41                         | 40                         | 0.98            | 1.27   |
| ISOHDFS60              | 7400  | 1.23       | 20.63 | 2.73                         | 44                         | 3.69            | 2.42   |
| ISOHDFS62              | 3720  | 0.73       | 20.67 | 2.54                         | 62                         | 0.95            | 1.19   |

<sup>1</sup>in units  $10^{-16}$  erg  $\text{cm}^{-2}\text{s}^{-1}$

<sup>2</sup>L( $H_\alpha$ ) in units  $10^{42}$  ergs<sup>-1</sup>

<sup>3</sup>L(FIR) in units  $10^{45}$  ergs<sup>-1</sup>

<sup>4</sup>no emission line detected

<sup>5</sup> $H_\alpha$ + $[NII]$  emission resolved.  $H_\alpha$  and  $[NII]$  fluxes and EWs are reported separately.

Table 2. Star Formation Rates

| name      | SFR( $H_\alpha$ )          | SFR(FIR)               |
|-----------|----------------------------|------------------------|
|           | uncorrected for extinction | based on FIR estimates |
| ISOHDFS16 | 1.5                        | 14                     |
| ISOHDFS23 | 1.2                        | 65                     |
| ISOHDFS25 | 3.5                        | 52                     |
| ISOHDFS27 | 3.6                        | 42                     |
| ISOHDFS28 | 0.8                        | 20                     |
| ISOHDFS38 | 18                         | 600                    |
| ISOHDFS39 | 52                         | 160                    |
| ISOHDFS53 | 7.0                        | 40                     |
| ISOHDFS55 | 5.0                        | 33                     |
| ISOHDFS60 | 18.5                       | 63                     |
| ISOHDFS62 | 4.8                        | 31                     |

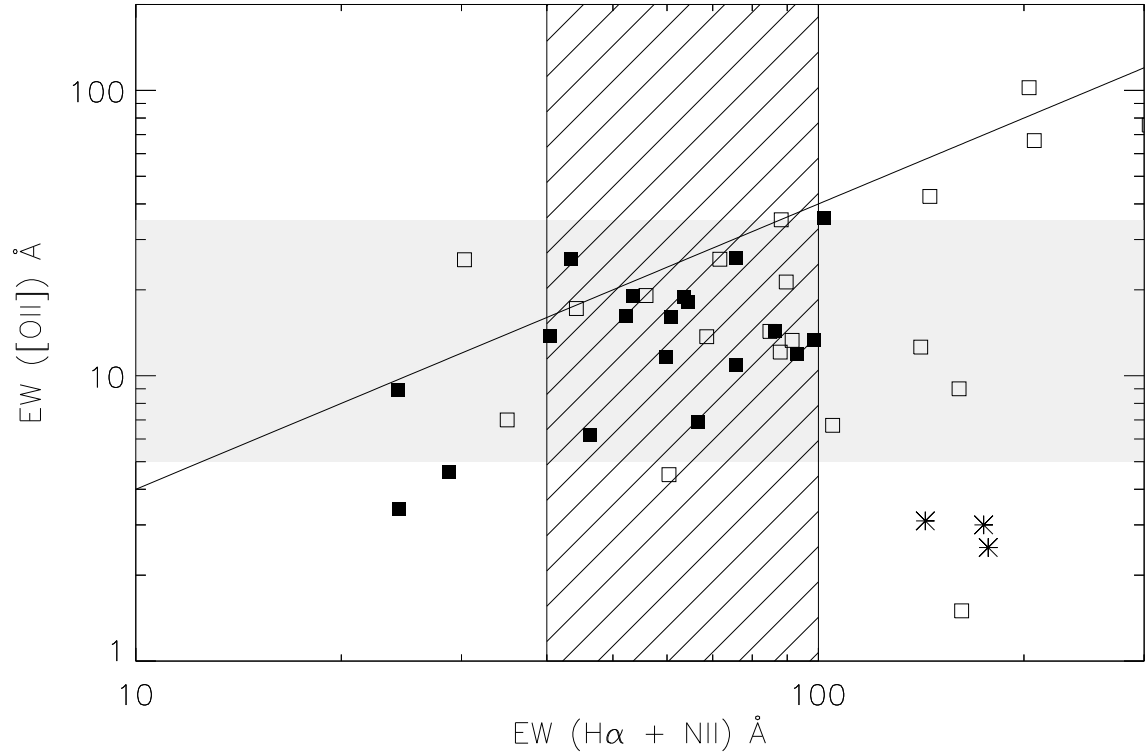


Fig. 2.—  $EW(OII)$  vs.  $EW(H\alpha + NII)$  diagram (from Poggianti and Wu (2000), filled squares e(a) galaxies, open squares non-e(a) galaxies, stars Seyferts). The black line corresponds to  $EW(OII) = 0.4 \cdot EW(H\alpha + NII)$  found for nearby field galaxies by Kennicutt 1992. The shaded bars represent the area of the VLT ISOHDFS galaxies. The intersection of the two bars is the location of our galaxies, indistinguishable from the dusty luminous e(a) galaxies.